Sandia National Laboratories
Albuquerque, New Mexico 87185

date: September 26, 2024

to: Distribution

from: Edmundo Corona (1558)

subject: Validation Exercise of a Coarse Finite Element Model of Laser Welds

Introduction

The objective of this project is to validate low-fidelity models of 304L to 304L stainless steel partial-penetration laser welds for thin sheets. Low-fidelity means that the weld is represented by coarsely meshed element blocks. Here, the hexahedral element size is approximately half the weld penetration depth. The material behavior of the block is represented by a J_2 plasticity model with a Voce hardening function.

The source of the data used in this work is an extensive experimental study conducted by Sharlotte Kramer (1528) and published in 2015 [1]. Figure 1 shows a cross-section of the weld of interest. The nominal thickness of the sheets is 0.063 in. while the target penetration depth of the weld is in the range of 0.028 to 0.032 in., extending about half the sheet thickness. Uniaxial tension tests provided data for calibration of base material and weld models. Results of two validation geometries were also provided. The principal validation geometry is shown in Fig. 2. It consists of a plate specimen with in-plane dimensions 6 in $\times$ 2.875 in loaded in tension. A circular plug with a 1.5 in. diameter was cut from the center of the plate and then welded in place. The details of the welding schedule are given in [1]. An important assumption is that the welds in the calibration and validation specimens have similar geometric and material properties as those in the validation tests.

The task was to first calibrate models for the base material and the welds and then simulate the validation tests until the point of weld first failure.

Model Calibrations

The work in [1] included uniaxial tension tests conducted on flat dog-bone specimens of the base 304L stainless steel material. The test section in the specimens had length and width

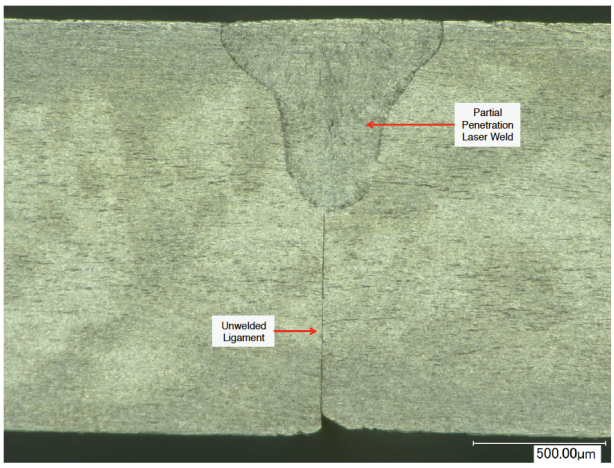

Figure 1. Cross-section showing the partial-penetration laser in the axial-thickness plane of a specimen (from [1]).

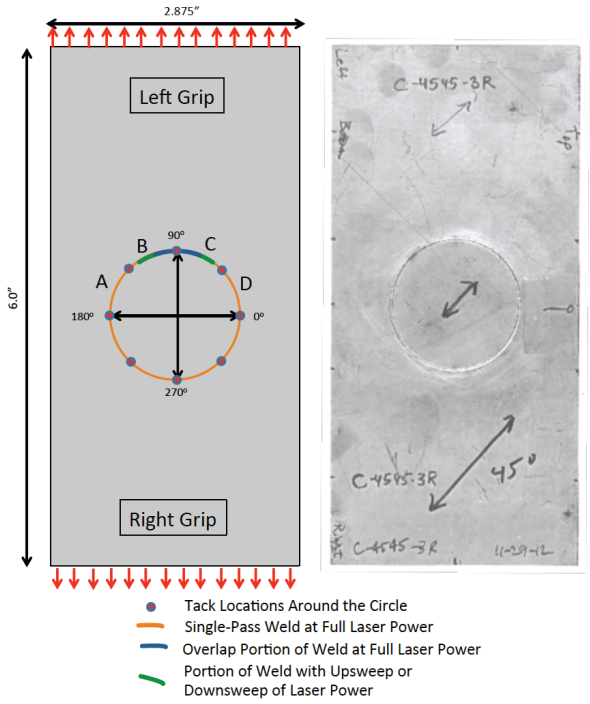

Figure 2. Validation specimen with circular weld (from [1]).

of 1.375 and 0.25 in., respectively, and thickness equal to that of the stock. An extensometer with a one-inch gage length measured the engineering strain. The results are shown in Fig. 3. The labels 'Axi', 'Per' and 'D45' refer to the orientation of the axis of the specimens being in the rolling direction, perpendicular to it, or at 45°. The 'Axi' specimens show slightly larger ultimate stress and lower strain to failure.

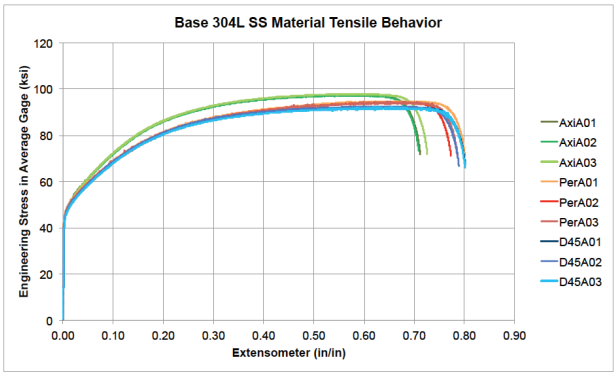

Figure 3. Uniaxial tension test results for the base material (from [1]).

Assuming that the effect of anisotropy in Fig. 3 is minor, the base material was represented using a rate and temperature independent J_2 plasticity model with a Voce hardening curve

$$\bar{\sigma} = \sigma_y + A(1 - e^{-n\bar{\varepsilon}^p}). \tag{1}$$

where $\bar{\sigma}$ and $\bar{\varepsilon}^p$ represent the equivalent stress and plastic strain and σ_y, A, n are parameters to be calibrated. Two of the curves in Fig. 3 were fit to represent specimens with high and low ultimate stress: AxiA02 and D45A03. The Voce parameters are given in Table 1. The Young's modulus E and Poisson's ratio ν were taken as 28.8×10^3 ksi and 0.28. The agreement between the test and simulation results is reasonably good up to a strain of 0.5, as shown in Fig. 4. Maximum equivalent plastic strains in the validation simulations were in the order of 0.25 in the sheets when the weld first failed.

Table 1. Voce parameters for 304L stainless steel sheet.

Test	σ_y, ksi	A, ksi	n
AxiA02	47	180	2
D45A03	45	170	2

Next, specimens with the same geometry, but containing a single weld at the mid-span of the test section were considered. The weld was perpendicular to the specimen length and spanned the width. These specimens were made by first welding two plates of dimensions 4 in × 3 in to make a single plate. The calibration specimens were then machined out of the welded plate. Figure 5 shows the resulting load-deflection curves, where the deflection was measured by a one-inch extensometer centered with respect to the weld. As expected, the results exhibit scatter in maximum load and failure displacement. The scatter in the

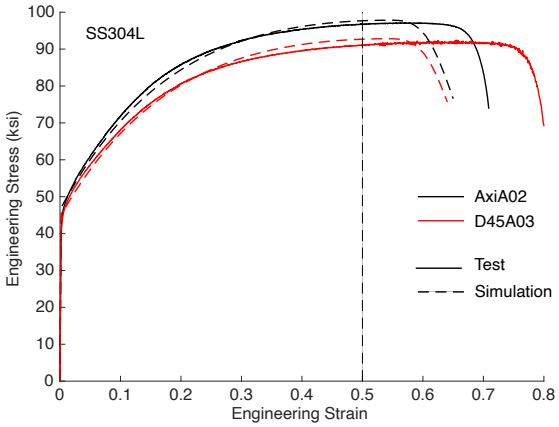

Figure 4. Comparison of observed and simulated uniaxial tension responses of 304L stainless steel sheet.

displacement to failure is approximately ±22% about the mean. The scatter can be partially correlated to the orientation of the specimen, but it is significant even within each orientation.

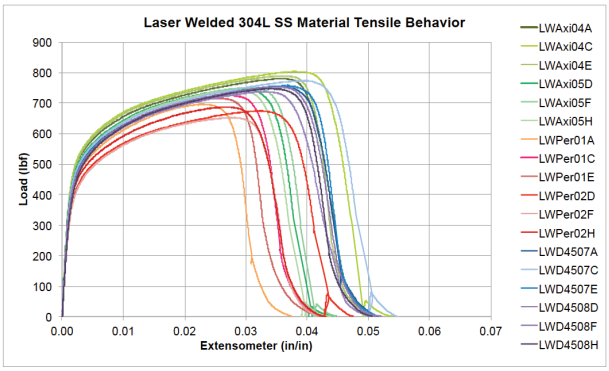

Figure 5. Load-deflection responses of narrow weld calibration specimens (from [1]).

Three of the curves were then selected for calibration, as shown in Fig. 6. The calibration was then conducted by simulating the tests using a finite element model of the specimens. A plan-view of the mesh used is shown in Fig. 7(a), and the deformed edge view is shown magnified in Fig. 7(b). The model of the weld is particularly important and introduced here.

- The weld is represented by a material block that has 4 elements through the weld cross-section in the edge view.
- Aside from this weld block, the material parameters are those of 304L stainless steel as given in Table 1 depending on the orientation of the specimen.

- The weld block is meshed continuously with the block representing the sheets over the vertical lines of nodes but not over the horizontal ones as is clearly seen in the figure.

These details are important because the weld model must have the same representation when it is applied in the validation cases.

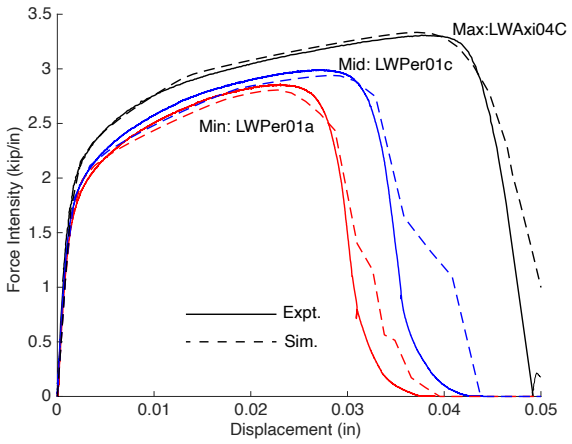

Figure 6. Load-deflection responses of selected narrow weld calibration specimens and simulation results.

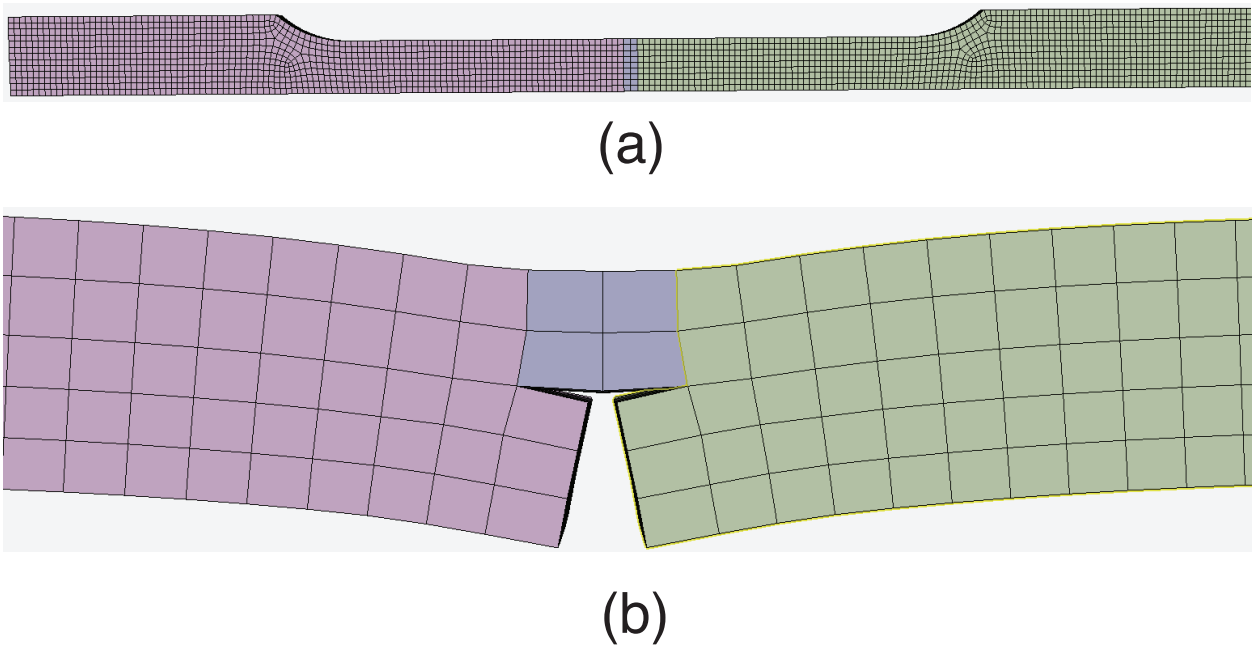

Figure 7. Mesh for calibration specimen. (a) Plan view and (b) edge view of deformed weld area.

Equally important are the initial dimensions of the block, which in this case are 0.034 in. in width and 0.028 in. in depth through the thickness. These values also have to be maintained

Table 2. Weld block Voce parameters.

Case	σ_y, ksi	A, ksi	n	$\bar{\varepsilon}_f^p$	ε_o	ε_k
Max	140	72	5	0.105	0.2	0.2
Mid	110	72	1	0.172	0.5	0.2
Min	102	72	1	0.172	0.5	0.2

in applications. This approach of modeling welds has been used previously [2]. The element size, and hence, the number of elements in the weld block is dictated by the specification of the minimum increment size in explicit dynamics calculations. Here it was chosen arbitrarily but within the range used in applications.

Since the Voce parameters of the base material are known, the properties of the weld block are assigned by comparing the results of simulations for the extensometer output to the test data. Voce fits in the J_2 plasticity model are also used to model the weld block material. It is also important to re-state that the geometry of the weld model remains constant, independently of the actual dimensions of the weld being modeled. The weld penetration depth can have a significant effect on the measured response but the resulting scatter is accommodated by the material properties of the weld block, not by changes in geometry. This approach is preferred given the coarse representation of the weld and the reality that input files are much easier to modify than having to change the mesh.

The model for the weld block also includes a ductile failure criterion based on equivalent plastic strain. Failure of the material starts when the equivalent plastic strain reaches a value $\bar{\varepsilon}_f^p$ listed in Table 2. A linear strain decline with respect to an accumulated crack opening strain [3] begins at this value of strain. The slope of the decay is such that the stress reaches zero when the crack opening strain is ε_o, but the element is deleted from the mesh when the crack opening strain reaches a value of ε_k. Table 2 list values for both ε_o and ε_k.

Validation Test

Experiments

The tensile load vs. grip displacement responses obtained for 11 tests of specimens of the type shown in Fig. 2 are shown in Fig. 8. The quantity of interest in this work is the first peak in the curves, which corresponds to failure initiation in the weld. The test data shows a spread in grip displacements between approximately 0.09 and 0.13 in. with no apparent correlation to the specimen orientation with respect to the rolling direction.

Because the grip displacement is usually affected by the compliance of the loading apparatus, it is better to make relative displacement measurements between points in the specimen. The displacement field over the whole specimen obtained by digital image correlation (DIC) was obtained for test C-4545-3. From there, the displacements at points 1 through 14 in Fig. 9 were extracted to define a series of virtual extensometers whose output can be compared between experiment and simulation.

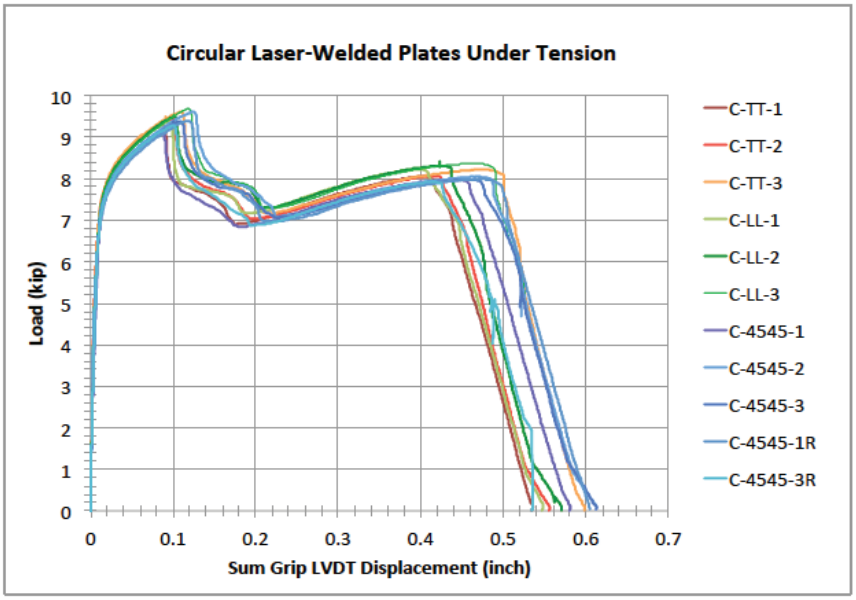

Figure 8. Load-deflection responses of all specimens with circular welds (from [1]).

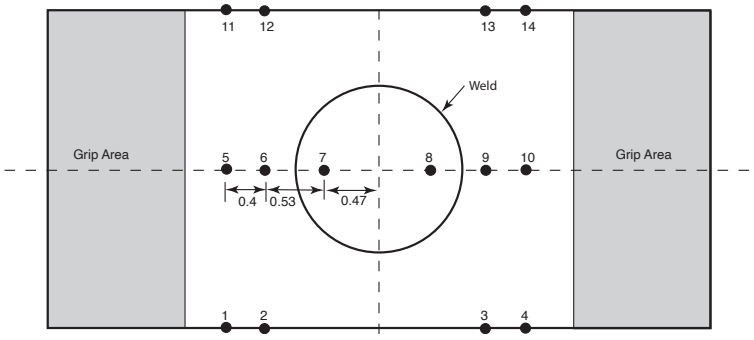

Figure 9. Displacement measurement points for circular weld.

Figure 10(a) shows the applied force vs. relative displacements across the weld between points indicated in the insert, as measured from the test data. The grip displacement curve is shown in black. Fracture of the weld initiated on the right while the left part of the weld did not fail. Hence, the red line continues accumulating displacement as the grips are pulled further apart and the crack opens. The blue line, on the other hand, shows a linear behavior suggesting unloading of that part of the weld. Figure 10(b) shows plots of the force divided by the specimen's cross-sectional area versus the normalized relative axial displacements in the specimen that do not span the weld, as shown in the insert. Normalized simply means that the relative displacement has been divided by the original distance between the points. After the load peak, the locations at the center-line unload as the load drops, and so do the locations on the edge of the specimen on the left. The edge locations to the right of the weld continue to stretch. Once the driving force to propagate the crack decreases significantly, the load increases again, but the center-line of the specimen does not stretch very much. The edges of the specimen stretch plastically until the sheets fracture along the width and the load drops to zero.

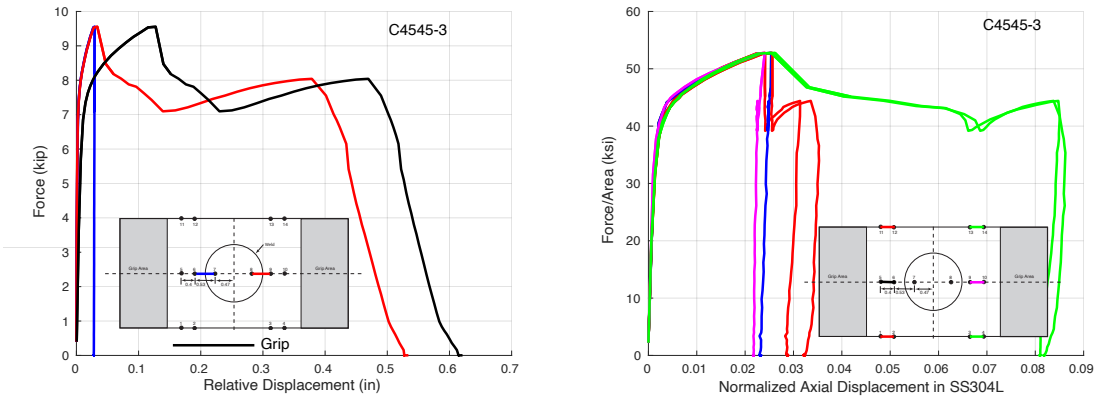

Figure 10. (a) Force-relative-displacement responses for the points indicated in the insert and (b) normalized force-relative-displacement responses at 6 locations not spanning the weldin the 304L stainless steel.

Simulations and Validation

The simulations were conducted with the finite element model shown in Fig. 11 that models one-half of the specimen in view of the one plane of symmetry along the specimen. The sheets are assigned the material D45A03 since the axis of the specimen was oriented at 45° to the rolling direction. Simulations have been conducted with all three sets of parameter models for the weld. The weld cross-section in Fig. 11(b) has the same dimensions and mesh as in the calibration experiments. The block, however, is divided into two parts: the 90° arc on the right and the one on the left, as can be seen in Fig. 11(a). Whereas both blocks had the same elastic-plastic parameters, only the right half of the block used a failure criterion to accommodate that experimental observation that failure occurred only on the right half of the weld. In addition to the symmetry boundary condition, the left edge of the

model was fixed in all directions whereas the right edge was fixed in the out-of-plane and transverse directions while the axial displacement was prescribed. The calculations were conducted using implicit quasi-statics up until the point where the numerical procedure ceased to converge.

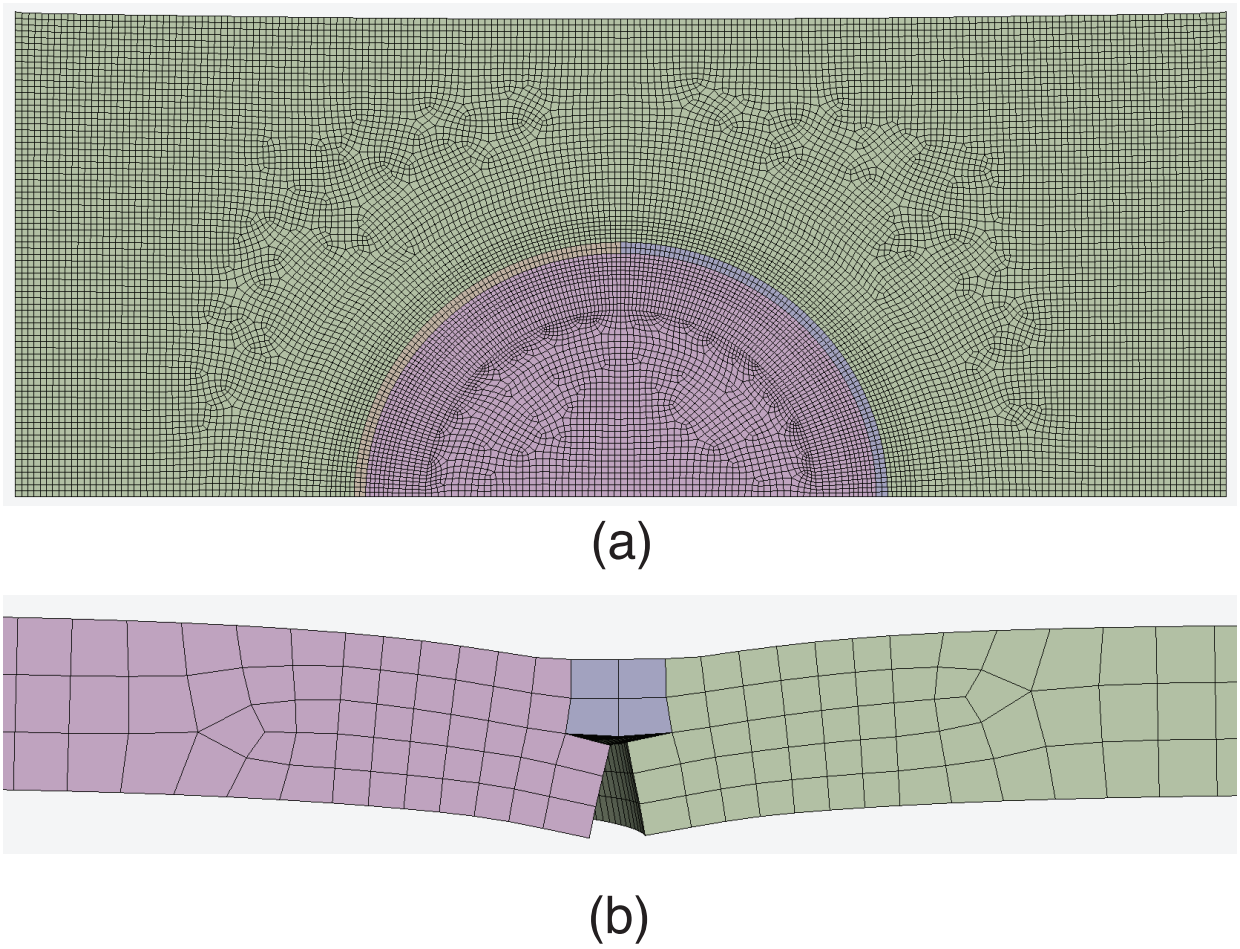

Figure 11. Mesh for specimen with circular weld. (a) Plan view and (b) edge view of deformed weld area.

Figure 12 shows the results of the calculations. The case 'Max' is shown in Figs.12(a) and (b) for the force-displacement curves across the welds and for the relative displacements in the sheets. In this case the maximum number of cutbacks (10) was reached in the adaptive step algorithm. The stress decay in the first element to reach the failure criterion started at a grip displacement of 0.064 in. and at the time where convergence failed, at a displacement of 0.14 in., elements had reached the death criterion and had to be deleted, causing the numerical solver to not converge. Comparing the relative displacements across the weld between experiment and simulation, the agreement up to weld first failure displacement is very good, with the analysis overestimating the failure displacement by just a small fraction. Note that the relative displacements between points in the sheets also exceed the experimentally

measured failure values.

Figures 12 (c), (d) and (e), (f) show similar results for the 'Mid' and "Min' weld fits, respectively. As expected the curves display failure at earlier displacements. Note that in these cases, the numerical procedure shows a sharp decrease in load starting at 0.088 in. in the 'Mid' case when elements begin to be deleted. The displacements in the sheets also follow the expected decreases and the trends in the experiments where the relative displacements in green line continue to increase while all the others show elastic unloading.

Using the grip displacement, the range of displacements at first weld failure can be compared to the test data. The range in the experiments was [0.09 in, 0.13 in] while the range in the simulations was [0.07 in, 0.14in]. The range from the simulations envelops that from the experiments and, as a percentage of the experimental limits, can be expressed as [78%,108%], a very good result considering the approximations in the model.

Next, the immediate post-peak response of the model is investigated for the 'Mid' case. In order to accomplish this, an explicit dynamics procedure is used. The advantage of this procedure is that, as long as the material models converge and elements are not inverted, the procedure easily powers through element death. The disadvantages are that it is a dynamic procedure that can be influenced by inertial loads and that the step size is very small, so orders of magnitude more steps are required compared to the quasi-static procedure. The idea here is then to apply the loads very smoothly with respect to time and over a period of time that is short enough to obtain a solution in a reasonable amount of time, but long enough that the contribution of inertia remains small. Here, a time period of 10 ms for a grip displacement of 0.4 in. was used.

The results are shown in Fig. 13. Differences between the experimental and the simulation results exist. The principal one is the more gradual drop in the load observed in the experiment. This is is likely an indication that the propagation of the crack along its circular path was more gradual in the experiments. In the simulations, the load drop is very sudden and the fracture propagates 90° degrees rather quickly. Once the fracture has propagated to its full extent, however, the load rises again and asymptotes towards the experimental measurements. Disagreement between experiment and simulation for crack propagation, however, is not surprising since no data addressing fracture propagation along the length of the welds was used in the model calibration. It must be highlighted that the calibration of the stress decay associated with failure in the weld block was loosely carried out and not properly optimized (due to lack of relevant data).

Second Validation Test

A second validation test, perhaps less demanding of the model, was conducted. This tests consists of a plate with the same outer dimensions as the circular weld test, but in this case the weld is straight across the width of the specimen, as shown in Fig. 14. The plate is subjected to tension along its long side. Figure 17 shows the experimental results in terms of load vs grip-displacement plots. Significant spread in the failure displacement plots can

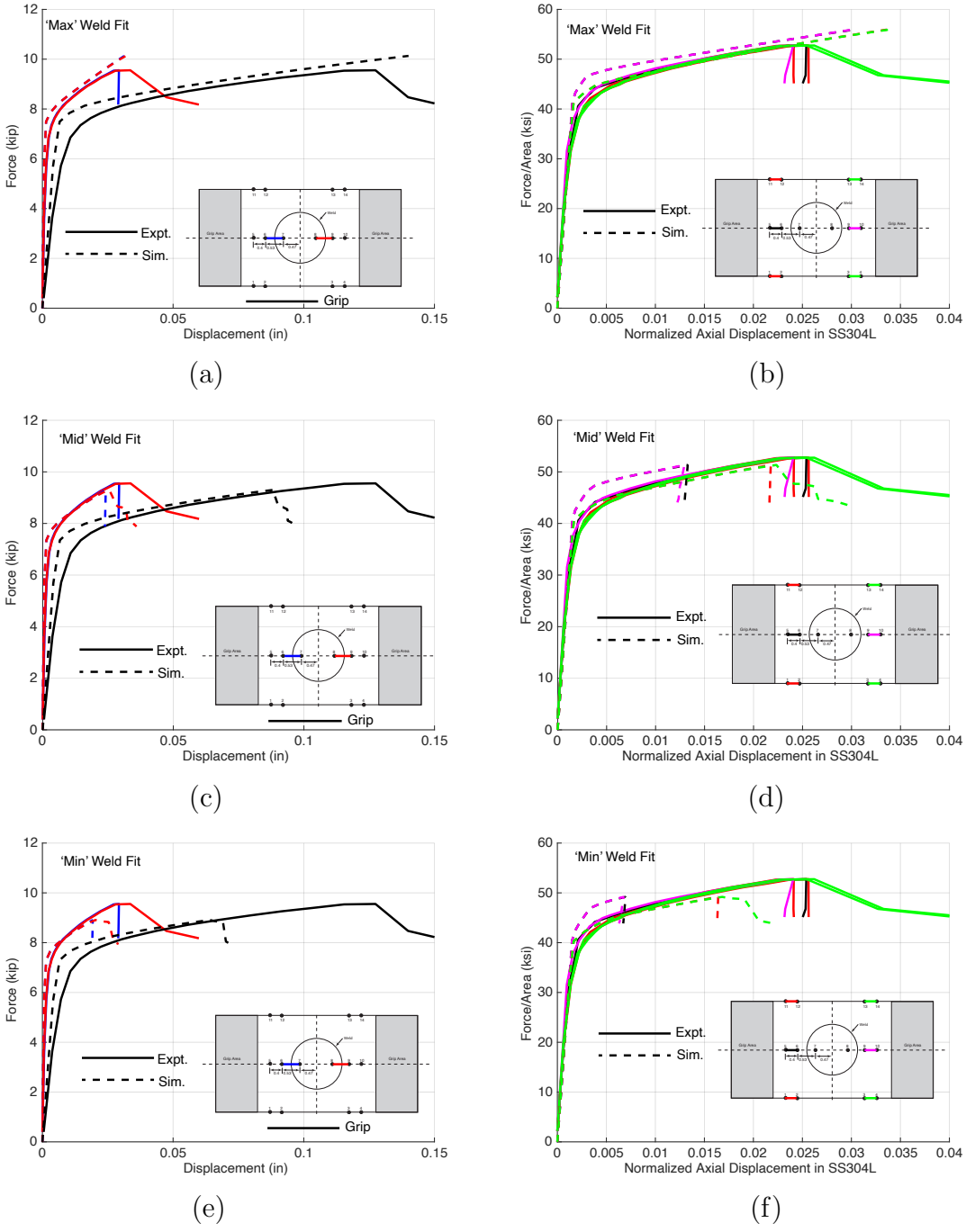

Figure 12. Experimental and explicit simulation results of plate specimen with circular weld with all three weld calibrations. (a) and (b): 'Max,' (c) and (d) : 'Mid,' (e) and (f) : 'Low.'

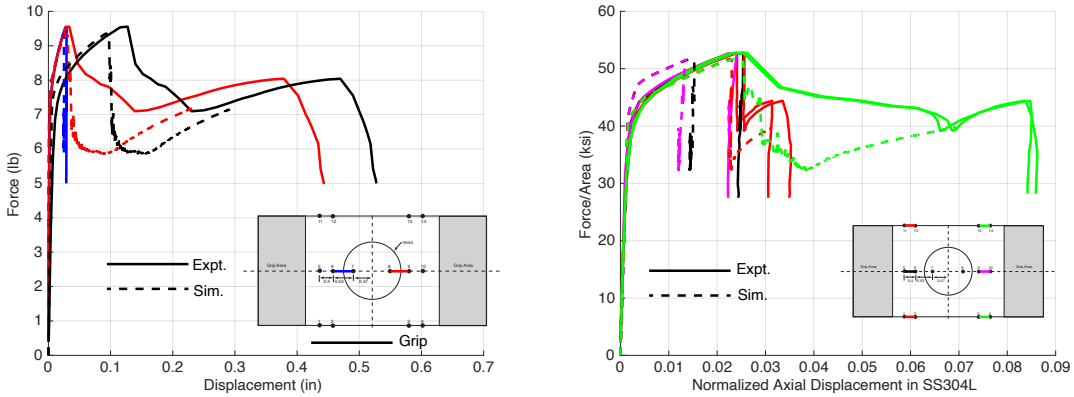

(a) (b)

Figure 13. Experimental and implicit simulation results of plate specimen with straight weld. (a) Force-displacement responses across the weld and (b) force-displacement responses in 304L stainless steel.

be seen that reflect the trends seen in the calibration tests. The specimens pulled along the rolling direction have significantly larger displacements to failure. As a whole, the range of the displacements to failure is [0.045 in, 0.12 in].

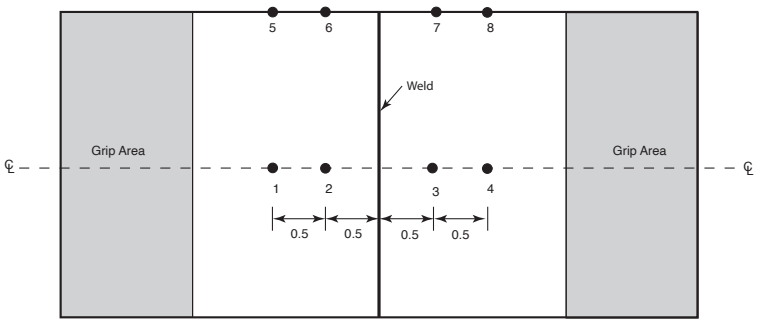

Figure 14. Displacement measurement points for the straight weld specimen.

A similar analysis effort as with the circular welds, but using the mesh in Fig. 16 was conducted for the test Plate29-LL, and the resullts are shown in Fig. 17. In general, the trends of the results are all very similar to those for the circular weld. The predicted grip displacements are in the range [0.4 in, 0.12in] which envelope the experimental values. One must be careful, however, by noting the different slopes of the curves for the grip displacement. If the compliance effects in the experiments was subtracted the range in the experiments would fall at lower displacement values.

One aspect common in model validation studies is an element size sensitivity study. In the present simulations, the calibration of the weld block was element size specific, so this block's mesh cannot be changed unless a whole new recalibration of the models is undertaken. Here, only the element size in regions away from the weld may be varied. Figure 18 shows results for 3 and 5 elements through the thickness of the sheets and the 'Mid' weld properties. The

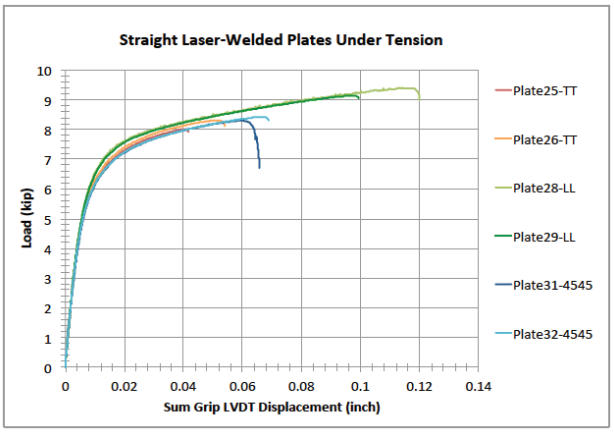

Figure 15. Load-deflection responses of all wide specimens with straight welds (from [1]).

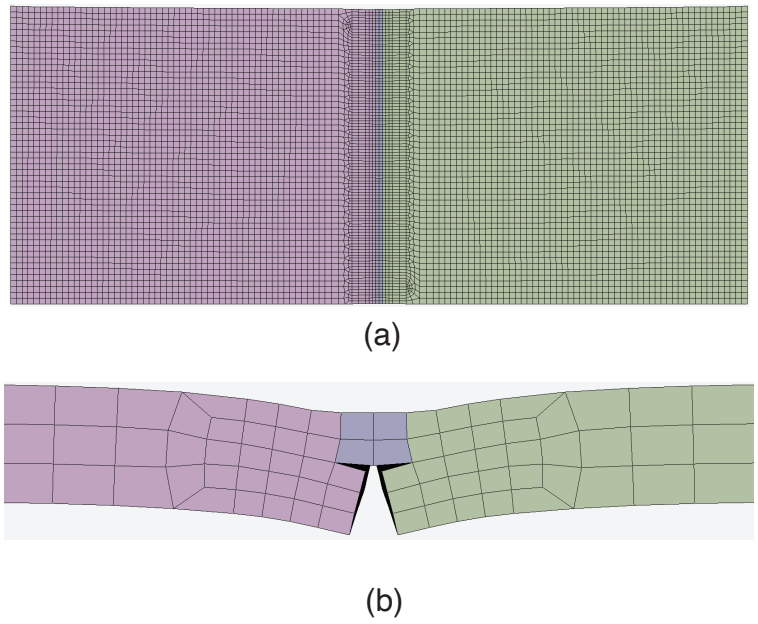

Figure 16. Mesh for specimen with straight weld. (a) Plan view, 3 for elements through plate thickness and (b) edge view of deformed weld area.

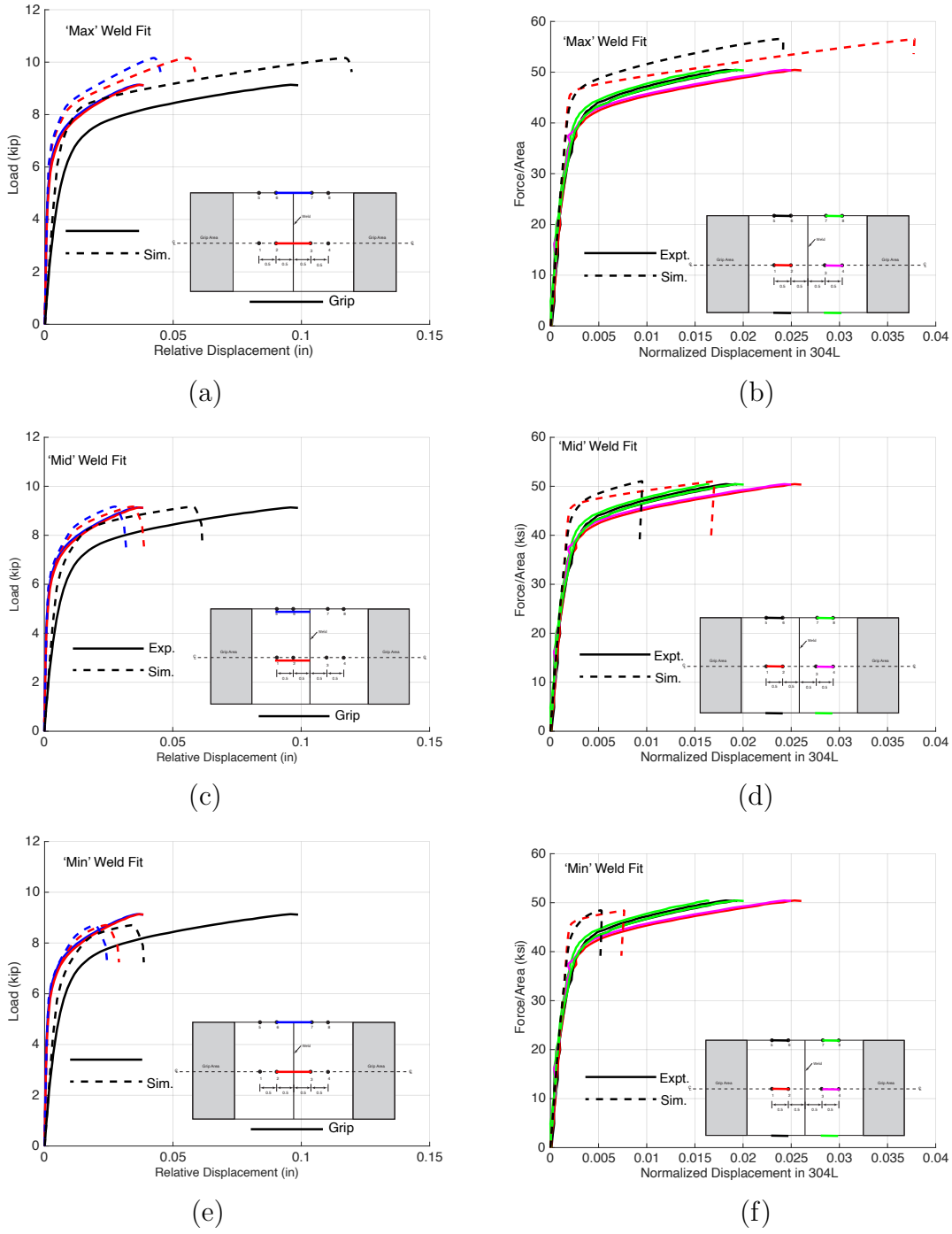

Figure 17. Experimental and explicit simulation results of plate specimen with straight weld with all three weld calibrations. (a) and (b): 'Max,' (c) and (d) : 'Mid,' (e) and (f) : 'Low.'

results of the simulations are essentially the same. Comparisons between 2 and 3 elements through the thickness for the circular welds also showed very small differences.

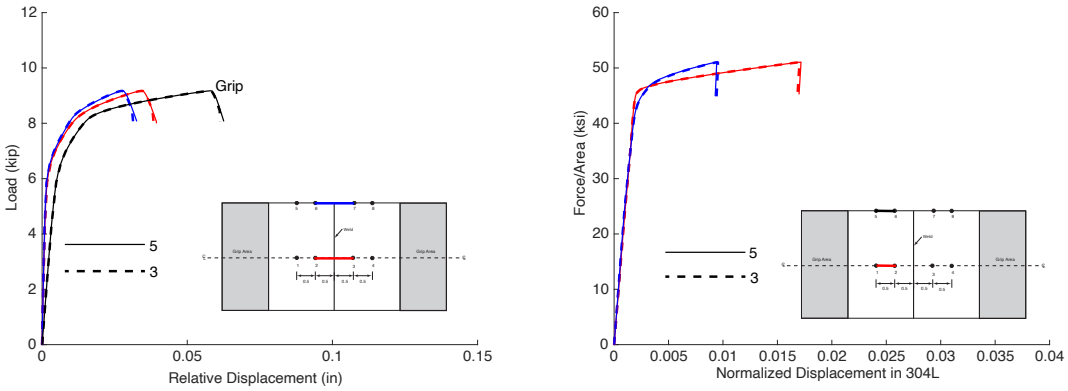

Figure 18. Results for 3 and 5 elements through thie thickness. (a) Simulation force-displacement responses across the weld and (b) normalized plot of responses within the 304L stainless steel.

Credibility Comments

A credibility exercise was conducted after the results of the report had been generated to practice the assessment of model credibility as outlined in [4].

Define Mathematical Description: The model can be described as a classical mechanics representation of kinematics and momentum balance as approximated by the finite element method. The material behavior approximations are based on the J_2 theory of plasticity and material failure depends on the accumulated equivalent plastic strain.

Identify Mathematical Model Input Parameters: They include the geometric parameters of the problem, in this case the overall dimensions of the specimen and the description of the weld block. The weld block is approximately the size of the actual weld, but does not replicate the actual weld geometry. Material parameters include the density when using explicit dynamics formulations as well as the parameters of the elastic-plastic models used to represent the base material and the weld block material. The geometric parameters were obtained from drawings in [1]. The material model parameters were obtained based on load-deflection curves of specimens with and without welds also provided in [1]. Welded specimens exhibited moderate variability in their load-deflection responses, so a range of material parameters were chosen to span the observed variability.

Perform a Numerical Solution: The numerical solution is based on the finite element method as implemented in the Sierra/SM code [5].

Code Solution and Output: The geometry and finite element mesh were created using Cubit. Fitting of the material data was conducted using finite element models of the calibration test specimens and varying the parameters of the plasticity and failure models manually until a reasonable approximation was achieved by visual comparison of the simulation and test results. Post-processing of the calibration and validation tests included visualization with Ensight and plotting of load-deflection curves via Matlab scripts.

V&V/UQ Activities: An important component of these activities is the PIRT table shown in Fig. 19.

Validation: The objective of this project was to validate the modeling method to determine when weld failure occurs when applied to the particular circular weld geometry presented in this memo. Hence, no prior validation exercise was conducted.

Uncertainty Quantification: The input parameters for the specimen geometries were kept fixed in both calibration and validation exercises because they are considered to be of medium importance. In particular, the actual geometry of the weld was substituted by a rectangular element block of nominal dimensions that remained unchanged in this work. Variations in the geometries of the actual welds were absorbed into the variability of the material parameters assigned to the block. The variation was determined by fitting test data from low, mid and high load-deflection responses of the weld calibration specimens. Finally, the properties of the base material were adjusted based on the orientation of the specimen with respect to the rolling direction of the sheets, but were otherwise kept fixed. The PIRT table provides a visual cue for the importance and adequacy of the model.

Code and Solution Verification: The Sierra/SM code and material library LAME have undergone daily verification testing for several years. Trust has been placed that this process guarantees the correct solution of the field equations and constitutive models. The work here presents a special case for the solution verification in terms of mesh refinement studies. The reason is that the method used to apply the calibration of the weld models requires that the element size in the weld blocks be the same in calibration and application. As a result, the mesh in the weld block was fixed and could not be changed. Only the mesh away from the weld block was modified for the straight weld specimen because it undergoes larger bending deflections that could be affected by the discretization. The sensitivity to the mesh density was small for the cases considered.

Conclusions

Low-fidelity modeling of welds is a current need in structural simulations at the component or system levels. This work considered validation exercises for 304L to 304L partial-penetration

ID	Phenomena	Importance	Adequacy for Intended Use				Comments
			Math Model	Code	Validation	Model Parameter	
A	Geometry						
A1	Overall	M	H	H	H	M	Used nominal dimensions
A2	Weld	L					Weld geometry not represented. Low-fidelity, coarse weld model
B	Base Material						
B1	Elastic-plastic behavior	H	H	H	M	M	Yield anisotropy not represented
C	Weld Material						
C1	Elastic-plastic behavior	H	H	H	M	M	Homogeneous weld block
C2	Failure	H	H	H	M	M	Homogeneous weld block

Figure 19. PIRT.

laser welds using a technique where the weld is substituted by a coarsely meshed block of hexahedral elements [2]. The material model for the base and weld block are both J_2 plasticity with Voce hardening and a critical equivalent plastic strain for ductile failure. The two validation exercises were: A plate with an in-plane circular plug welded at the center, and a plate with an edge-to-edge weld joining the two plate halves oriented perpendicular to the applied load direction.

- In general the calibration/validation exercises were successful determining first failure of the welds. It was important define virtual extensometers based on the DIC data from two tests to successfully correlate the test and simulation results.
- After first failure in the circular weld case, the load dropped precipitously in the simulations, but more gradually in the tests. This is likely related to a more gradual crack propagation in the tests. The models, however, were not calibrated for fracture propagation, and the focus of this work was on the initiation of failure.

Acknowledgments

Thanks go to Sharlotte Kramer, Brian Lester and Kyle Karlson for useful discussions on the subject of this report. The assistance of Matthew Swanson providing the DIC data from the validation experiments is also acknowledged with thanks.

Figures 1, 2, 3, 5, 8, and 15 were copied from [1]. A thank-you goes to Sharlotte Kramer for giving permission to use them in this report.

Sandia National Laboratories is a multimission laboratory managed and operated by National Technology and Engineering Solutions of Sandia, LLC, a wholly owned subsidiary of Honeywell International Inc., for the U.S. Department of Energy's National Nuclear Security Administration under contract DE-NA0003525.

References

[1] Kramer, S.L.B., Characterization of 304L stainless steel laser welds, SAND2015-9012.

[2] Corona, E., Jones, A.R., Kramer, S.L.B., Fietek, C.J. and Lester, B.T., GTA and laser weld mechanical testing and model calibrations for elastic-plastic deformation and failure, SAND2023-06306.

[3] Vignes, C. and Lester, B., Modification of tearing parameter failure for anisotropic plasticity, Sandia Technical Memo SAND2023-14193R.

[4] Dowding, K., General engineering documentation , modeling & simulation and credibility framework. Personal communication.

[5] Sierra Solid Mechanics Team, Sierra/SolidMechanics 5.4 user's guide. SAND2022-0103, 2022.

Internal Distribution:

A. Jones	1528
S. Kramer	1528
M. Swanson	1528
J. Emery	1556
B. Lester	1558
S. Nelson	1558
D. Reedy	1558
K. Karlson	8752
J. Zaine	8752